

Comparison of *PARASOL* Observations with Polarized Reflectances Simulated Using Different Ice Habit Mixtures

BENJAMIN H. COLE AND PING YANG

Department of Atmospheric Sciences, Texas A&M University, College Station, Texas

BRYAN A. BAUM

Space Science and Engineering Center, University of Wisconsin—Madison, Madison, Wisconsin

JEROME RIEDI, LAURENT C.-LABONNOTE, AND FRANCOIS THIEULEUX

Laboratoire d'Optique Atmosphérique, UMR CNRS 8518, Université de Lille 1—Sciences et Technologies, Villeneuve d'Ascq, France

STEVEN PLATNICK

NASA Goddard Space Flight Center, Greenbelt, Maryland

(Manuscript received 30 March 2012, in final form 27 June 2012)

ABSTRACT

Insufficient knowledge of the habit distribution and the degree of surface roughness of ice crystals within ice clouds is a source of uncertainty in the forward light scattering and radiative transfer simulations of ice clouds used in downstream applications. The Moderate Resolution Imaging Spectroradiometer (MODIS) collection-5 ice microphysical model presumes a mixture of various ice crystal shapes with smooth facets, except for the compact aggregate of columns for which a severely rough condition is assumed. When compared with *Polarization and Anisotropy of Reflectances for Atmospheric Sciences coupled with Observations from a Lidar (PARASOL)* polarized reflection data, simulations of polarized reflectance using smooth particles show a poor fit to the measurements, whereas very rough-faceted particles provide an improved fit to the polarized reflectance. In this study a new microphysical model based on a mixture of nine different ice crystal habits with severely roughened facets is developed. Simulated polarized reflectance using the new ice habit distribution is calculated using a vector adding–doubling radiative transfer model, and the simulations closely agree with the polarized reflectance observed by *PARASOL*. The new general habit mixture is also tested using a spherical albedo differences analysis, and surface roughening is found to improve the consistency of multiangular observations. These results are consistent with previous studies that have used polarized reflection data. It is suggested that an ice model incorporating an ensemble of different habits with severely roughened surfaces would potentially be an adequate choice for global ice cloud retrievals.

1. Introduction

Ice clouds play an important role in regulating the energy balance of the earth (Liou 1986), with a frequency of occurrence approaching 70% in tropical regions (Nazaryan et al. 2008). The ice cloud microphysics largely determines the radiative properties of these

clouds, but current knowledge of ice cloud microphysics is still limited (Baran 2009). Cloud modeling and comparison with remote sensing observations can be used to investigate the properties of ice clouds and reduce uncertainties in their microphysical properties. In current operational ice cloud retrievals using the Moderate Resolution Imaging Spectroradiometer (MODIS) satellite, the collection-5 ice cloud model (Baum et al. 2005b) is used. This model consists of six different particle shapes (habits) and smooth surfaces for all the habits, except for the compact aggregate consisting of severely roughened solid columns. To improve the

Corresponding author address: Benjamin H. Cole, Dept. of Atmospheric Sciences, Texas A&M University, 3150 TAMU, College Station, TX 77843.
E-mail: ben.cole@tamu.edu

MODIS collection-5 model, a new ice model incorporating nine different ice habits with severely roughened facets is suggested in this study. In addition to the ice crystal habits in the MODIS collection-5 model, the new model incorporates three new ice habits: a hollow bullet rosette and a small and large spatial aggregate of plates.

Chepfer et al. (1998) showed that polarization is sensitive to the shape of the ice crystals. To examine the impact of the new ice model, simulations of polarized reflectance from an optically thick ice cloud ($\tau = 5$) are compared with *Polarization and Anisotropy of Reflectances for Atmospheric Sciences coupled with Observations from a Lidar (PARASOL)* multiangle polarized reflectance measurements. The adding–doubling model of de Haan et al. (1987) is employed to simulate the polarized reflectance at the top of the atmosphere (TOA). The single-scattering properties of the ice crystals were taken from a new database that provides the spectrally consistent optical properties of ice particles from ultraviolet to far-infrared wavelength regimes (Yang et al. 2013), and the bulk scattering properties are calculated following Baum et al. (2005b, 2011). In addition, a spherical albedo differences (SAD) analysis (Doutriaux-Boucher et al. 2000) is performed to investigate the angular consistency of the ice cloud model. The SAD analysis consists of inferring cloud optical thickness τ at various observation angles and subsequently testing the consistency of the cloud spherical albedo derived from these τ values.

The remainder of this paper contains the following sections. Section 2 outlines the data used and the radiative transfer (RT) model employed to perform the simulations for the polarized reflectance analysis, section 3 presents the results of the comparison of model simulations of polarized reflectance and the spherical albedo difference with *PARASOL* satellite measurements, and section 4 summarizes the work.

2. Data and models

a. The PARASOL satellite

PARASOL is a French microsatellite launched in 2004 to study clouds and aerosols with multiple angle and polarization capabilities (Fougnie et al. 2007). It carries a derivative of the Polarization and Directionality of the Earth's Reflectances (POLDER) instrument, a wide-field imaging radiometer and polarimeter. This instrument has nine bands, three of which have polarization capabilities. *PARASOL* views a given scene at up to 16 different angles as the satellite passes overhead. The polarization is achieved with filters at increments of 60° in a rotating-wheel assembly (Deschamps et al.

1994). The measurements provide the I , Q , and U Stokes vector components, from which both cloud and aerosol properties may be inferred.

In this study, the level-2 cloud product is used, which is based on the level-1B radiances averaged over a larger spatial area [$\sim(18 \times 18)$ km]. Included in this product is the fractional cloud cover, surface type, cloud thermodynamic phase (ice, water, or mixed), and normalized, modified, polarized radiance L_{nmp} at 865 nm. The radiance L_{nmp} is defined as follows (C.-Labonnote et al. 2001):

$$L_{\text{nmp}} = \frac{\pi L_p \cos\theta_s + \cos\theta_v}{E_s \cos\theta_s}, \quad (1)$$

where subscript s represents the solar zenith and azimuth angles and subscript v is the viewing angle. The E_s is the TOA solar irradiance. Since L_{nmp} is normalized by the incident irradiance, it is a dimensionless quantity, and will be called polarized reflectance in this paper. The term L_p is the linearly polarized radiance, defined as

$$L_p = \pm \sqrt{Q^2 + U^2}, \quad (2)$$

where the sign is determined by the angle between the polarization vector and the normal to the scattering plane (C.-Labonnote et al. 2001).

One full day of global *PARASOL* observations from 1 August 2007 are used in this study, representing 14 orbits. The product is filtered to retain *PARASOL* pixels over the ocean with 100% cloud cover within the $18 \text{ km} \times 18 \text{ km}$ spatial area. Additionally, the cloud phase indicated in the level-2 product must be ice, and there must be at least seven different viewing geometries observed by *PARASOL* for a given pixel to be included in this study. The total number of pixels before filtering was 933 129, with 69 481 pixels (just over 7%) remaining after filtering using the criteria described above. Of the pixels remaining after filtering, 14 241 are in the tropics and 55 240 are in the higher latitudes.

b. Adding–doubling radiative transfer model

The vector adding–doubling RT model developed by de Haan et al. (1987) is used to provide the intensity and polarization state of radiation at the TOA, containing a layer of modeled ice cloud with given scattering properties. A midlatitude summer atmospheric profile based on the *U.S. Standard Atmosphere, 1976* is used in the calculations, assuming a total Rayleigh optical depth of 0.01587 at 865 nm (Tomasi et al. 2005). All simulations assume a single-layer ice cloud with an optical thickness of 5 at a height of 9 km over an ocean surface with an index of refraction value of 1.33. The viewing

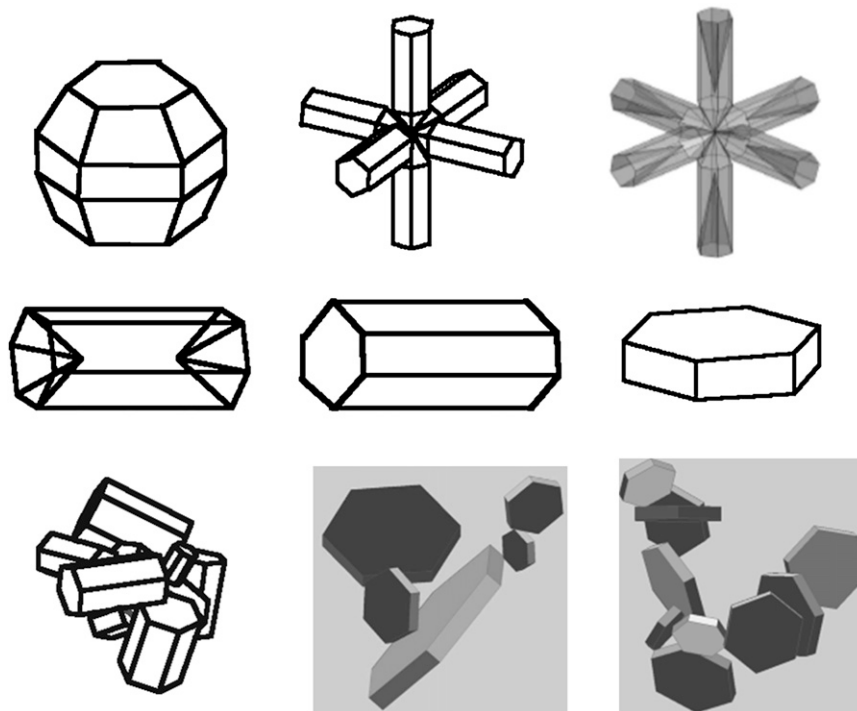


FIG. 1. The nine ice habits used in the general habit mix. The top row shows a droxtal plus solid and hollow 3D bullet rosettes, the middle row shows a hollow and a solid column and a plate, and the bottom row shows a compact aggregate of columns, a 5-member spatial aggregate of plates, and a 10-member spatial aggregate of plates.

geometries of 3000 randomly selected *PARASOL* pixels from 1 August 2007 are used as the input geometries to produce the simulated polarized reflectance. The selected geometries encompass the full range of scattering angles seen in *PARASOL* observations. The Stokes vector output at TOA is used to produce the simulated polarized reflectance L_{nmp} , the same quantity as from *PARASOL* observations.

c. Spherical albedo differences test

To test the angular coherence of cloud spherical albedo, a SAD analysis (Doutriaux-Boucher et al. 2000) is performed. The cloud optical thickness is derived from the different observation angles available from *PARASOL* and then the microphysical and optical properties in a chosen cloud model are used to infer the spherical albedo. This can be done since there is a one-to-one relationship between cloud optical thickness and spherical albedo (Doutriaux-Boucher et al. 2000) when a black underlying surface is assumed [for details on the *PARASOL* retrieval method, see Buriez et al. (1997)]. If the cloud model described the optical properties perfectly, the spherical albedo would be independent of scattering angle. Any differences observed between the multiangle retrievals of cloud spherical albedo provide

information about the angular consistency of the assumed cloud model. It is important to note that the cloud model actually includes two separate assumptions: one on cloud macrophysical properties (cloud is plane-parallel and homogeneous) and the other on microphysical properties (particle size and habit distribution). Both could potentially impact the angular distribution of reflectance, but it is assumed that the cloud microphysics (through the ice-phase function) is the dominant factor governing rapid changes in the cloud bidirectional reflectance distribution function (BRDF) and the bidirectional polarization distribution function (BPDF), especially when an analysis is performed over a wide range of view and sun zenith angles, and subsequently scattering angles. Additionally, the large sampling domain [$\sim(18 \times 18)$ km pixels] will mitigate the potential 3D cloud effects.

d. Ice bulk scattering properties

The calculation of the reflected polarized light using the adding-doubling model requires the bulk scattering properties of the ice particles within the simulated cloud. For this study, the single-scattering properties of nine different ice habits (shapes) are obtained at a wavelength of 865 nm with a combination of the discrete

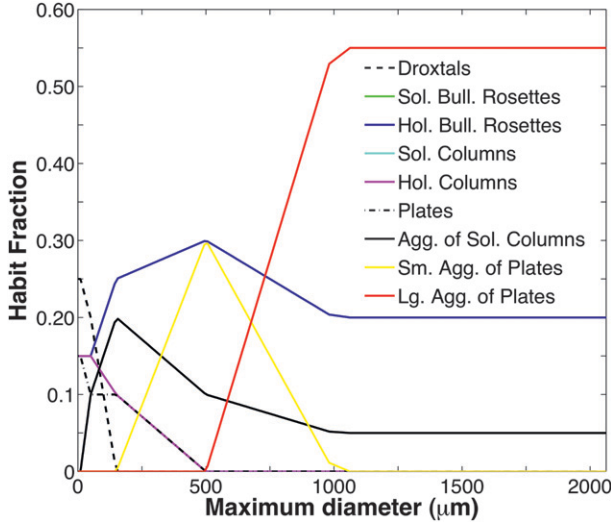


FIG. 2. Ice crystal habit fraction as a function of diameter for the general habit mix used in this study. The habit fractions remain the same past the maximum size shown in this plot. These fractions are used when calculating bulk scattering properties using measured particle size distributions.

dipole approximation method and the improved geometric optics method (Yang et al. 2013). The nine habits are droxtals, solid and hollow columns, solid and hollow 3D bullet rosettes, plates, a compact aggregate of columns, and a small and large spatial aggregate of plates, whose geometries are illustrated in Fig. 1. The

single-scattering properties are derived assuming random orientation of the particles. The ice particles may have smooth, moderately roughened, and severely roughened surfaces. The method for simulating the surface roughness is to randomly lift and tilt the facet of the ice particle. The parameter σ describes the level of roughness, with $\sigma = 0$ being smooth, 0.05 representing moderately roughened particles, and a level of $\sigma = 0.5$ for severely roughened ice particles (Yang and Liou 1998).

The procedure for calculating the bulk scattering properties follows that of Baum et al. (2005b, 2011). For an ice cloud composed of a mixture of habits, the bulk scattering properties are obtained from integration over the habit distribution, the size distribution, the spectral response function of the *PARASOL* imager, and the solar spectrum. The size distributions used in the calculations come from a variety of field campaigns including the Cirrus Regional Study of Tropical Anvils and Cirrus Layers–Florida–Area Cirrus Experiment (CRYSTAL–FACE), the Tropical Rainfall Measuring Mission (TRMM), the Atmospheric Radiation Measurement (ARM) Program, the Stratospheric–Climate Links with Emphasis on the Upper Troposphere and Lower Stratosphere (SCOUT) field campaign, and others (Baum et al. 2011).

The average single-scattering phase matrix is computed in the following way:

$$P(\Theta) = \frac{\int_{\lambda_1}^{\lambda_2} \int_{D_{\min}}^{D_{\max}} \left[\sum_{h=1}^M P_h(\Theta, D, \lambda) \sigma_{\text{sca},h}(D, \lambda) f_h(D) \right] n(D) F_s(\lambda) S(\lambda) dD d\lambda}{\int_{\lambda_1}^{\lambda_2} \int_{D_{\min}}^{D_{\max}} \left[\sum_{h=1}^M \sigma_{\text{sca},h}(D, \lambda) f_h(D) \right] n(D) F_s(\lambda) S(\lambda) dD d\lambda}, \quad (3)$$

where M is the number of habits, D is the particle diameter, $n(D)$ is the number density, $F_s(\lambda)$ is the spectral response function, and $S(\lambda)$ is the solar flux. The scattering cross section is σ , and the habit fraction is defined so that

$$\sum_{h=1}^M f_h(D) = 1. \quad (4)$$

The effective diameter D_{eff} is proportional to the ratio of the total volume to the total projected area and is given by the following expression:

$$D_{\text{eff}} = \frac{3 \sum_{h=1}^M \left[\int_{D_{\min}}^{D_{\max}} V_h(D) f_h(D) n(D) dD \right]}{2 \sum_{h=1}^M \left[\int_{D_{\min}}^{D_{\max}} A_h(D) f_h(D) n(D) dD \right]}. \quad (5)$$

The bulk asymmetry parameter g and bulk scattering cross sections are calculated in the same manner as the phase matrix above.

The resulting phase functions tend to be strongly peaked in the forward direction, making it necessary to truncate this peak before performing the radiative transfer calculations. The δ -fit method (Hu et al. 2000) is used to truncate the forward peak, and the other phase matrix elements are then normalized by the truncated phase function. The truncated, normalized bulk scattering phase matrix is then used in the RT calculations. In addition, the optical thickness, scattering cross section, and asymmetry parameter are all adjusted after the truncation based on the similarity principle (Joseph et al. 1976).

For this study, the habit distribution used in MODIS collection-5 retrievals is considered (henceforth referred

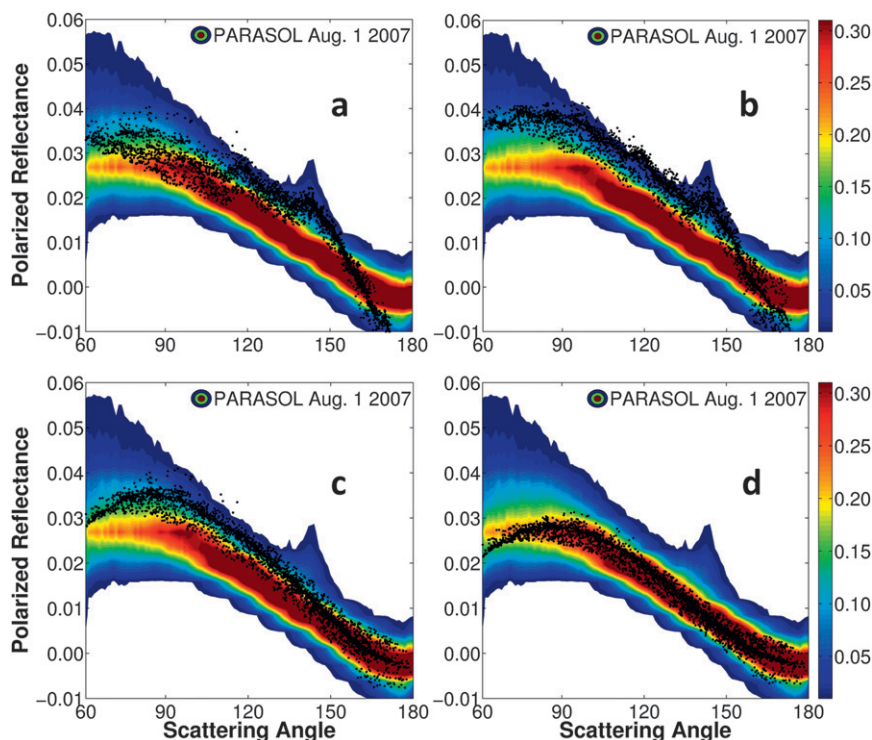


FIG. 3. Simulated polarized reflectance calculated at an effective diameter of $60 \mu\text{m}$ with an optically thick ($\tau = 5$) ice cloud for (a) the MODIS collection-5 model, (b) a general habit mix with smooth ice particles, (c) a general habit mix with moderately rough ice particles, and (d) a general habit mix with severely rough ice particles. Color contours show the density of the *PARASOL* polarized reflectance data from 1 Aug 2007, and black dots are simulations.

to as C5M), along with a general habit mixture (GHM) proposed for future MODIS retrievals. The single-scattering properties for the single habits used in the GHM are also used in simulations and the results are analyzed. The MODIS C5M includes the following six habits: solid columns, hollow columns, solid 3D bullet rosettes, droxtals, plates, and a compact aggregate of solid columns. Droxtals are used for the smallest sizes, while columns, plates, and bullet rosettes make up the middle sizes. Aggregates of solid columns and single solid bullet rosettes are used for the largest ice particle sizes in the size distribution considered. All of the ice habits considered are smooth surfaced in C5M, with the exception of the compact aggregate of solid columns, which is severely roughened.

In addition to the six habits in MODIS C5M, the proposed GHM includes 3D hollow bullet rosettes, and a small and a large spatial aggregate of plates. In contrast to the C5M, the habits transition linearly with particle size; this prevents potential artifacts in the bulk scattering properties that could arise from switching habits abruptly. Figure 2 shows the GHM distribution of habits as a function of particle diameter.

The intent is that a given habit distribution will provide results for inferred ice cloud optical thickness and particle size that are consistent between sensors taking measurements at different wavelengths. One way of assessing the consistency in the expected retrievals is to examine results using the polarized reflectance and total radiance measurements from *PARASOL*. In this study, the polarized and total radiances are simulated using the bulk scattering properties as input into an RT model, whereupon the simulated radiances are compared with those from *PARASOL*.

3. Results

In this section we present the results of simulations of polarized reflectance based on bulk scattering models derived using the C5M, the GHM, and selected individual habits. The simulations of polarized reflectance are compared to polarized reflectance measured by *PARASOL* on 1 August 2007. An optical thickness of $\tau = 5$ is assumed for all simulations so that the polarized reflectance is saturated. Figure 3a shows simulated polarized reflectance using the C5M assuming

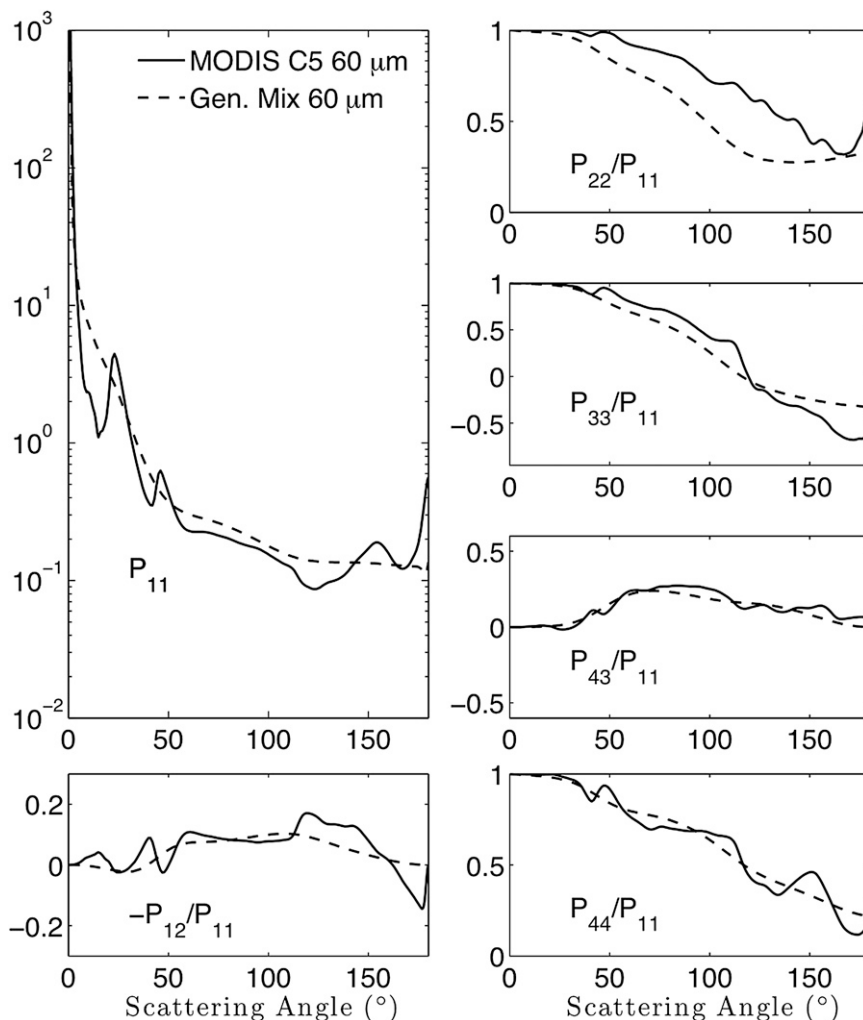


FIG. 4. Comparison of the phase matrix components of the MODIS collection-5 ice habit mix and the general habit mix with severe surface roughness at an effective diameter of $60 \mu\text{m}$.

$D_{\text{eff}} = 60 \mu\text{m}$ (black dots) superimposed over the measured polarized reflectances from *PARASOL* (color contours). The color contours represent the smoothed frequency of *PARASOL* measurements, with blue (red) displaying lower (higher) frequencies of observed reflectances. The black dots are based on a set of 3000 points defined by the viewing geometry from individual *PARASOL* pixels. Because the same scattering angle may be obtained from different combinations of viewing zenith, solar zenith, and relative azimuth angles, a given scattering angle may have several simulated polarized reflectance points; this leads to the dispersion in the simulation results seen in Fig. 3 and the following figures. The simulated reflectances for the C5M clearly do not match well with the measurements over the range of scattering angles.

Figure 3b shows the simulation results that are obtained if the GHM is adopted assuming smooth particles,

for the same conditions of $D_{\text{eff}} = 60 \mu\text{m}$ and $\tau = 5$. To be clear, the results assume smooth-faceted particles similar to the C5M but employ the additional three habits, and are based on linearly changing habit fractions. The results indicate that increasing the number of ice habits in the mixture and changing their fractions does not improve the comparison with the measured polarized reflectance data.

Another parameter to consider is surface roughness. Figure 3c shows the results for the GHM with a moderate level of surface roughness, once again with $D_{\text{eff}} = 60 \mu\text{m}$ and $\tau = 5$. Note that the peaks are smoothed out and the fit to observed polarized reflectance improves over that for smooth particles, but the values are still too high, especially for scattering angles from 60° to 130° .

Figure 3d shows the results for the GHM with severely roughened particles, once again with $D_{\text{eff}} = 60 \mu\text{m}$ and

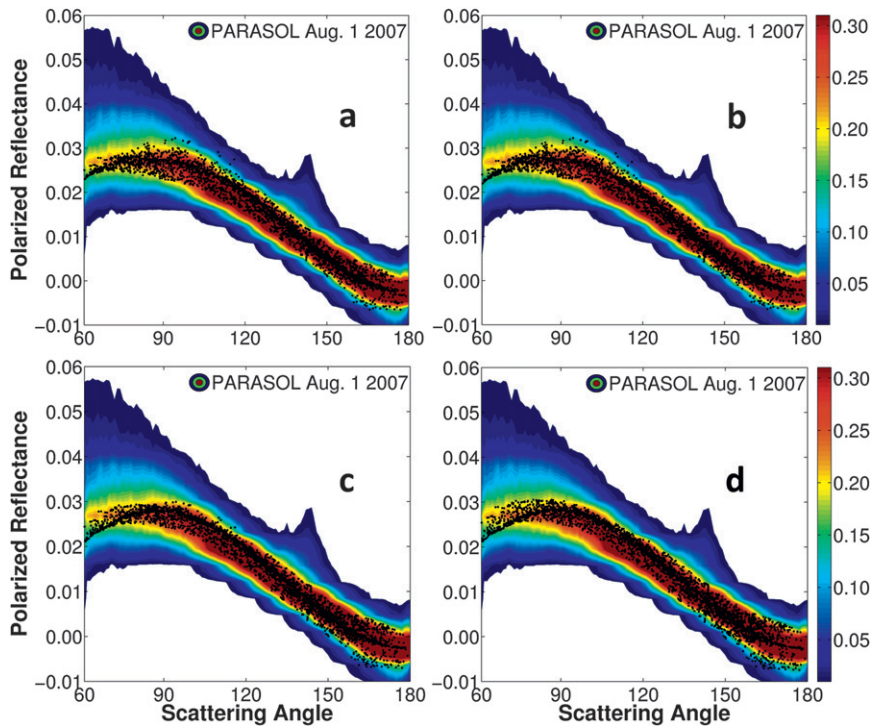


FIG. 5. Simulated polarized reflectance calculated using the general habit mix at four different effective diameters: (a) 30, (b) 50, (c) 70, and (d) 90 μm . An optically thick ($\tau = 5$) ice cloud is used in the simulation and the ice particles are severely rough. Color contours show the density of the *PARASOL* polarized reflectance data from 1 Aug 2007, and black dots are simulations.

$\tau = 5$. When severe surface roughness is used in the simulations, the simulated and measured polarized reflectances are much closer over the range of scattering angles. The severely roughened particles provide the closest fit to the observed polarized reflectances and indicate that the bulk ice cloud optical properties should incorporate at least a certain degree of surface roughness in their derivation.

The dramatic change in polarized reflectances observed in the simulations from particle roughening comes from the removal of peaks in the scattering phase matrix, as seen in Fig. 4. This influence on the polarized reflectance from smoothing of the phase matrix by inclusions or roughening was noted by C.-Labonnote et al. (2001) and Baran and C.-Labonnote (2006, 2007). As Fig. 4 shows, the phase function becomes nearly featureless when assuming severe surface roughness. The degree of linear polarization, P_{12} , becomes almost featureless as well, with a downward slope over the range of scattering angles observed from polar-orbiting sensors. This smoothing of the scattering phase matrix by the roughening of the ice surface is discussed in more detail in Baum et al. (2010).

Figure 3 showed that in comparison with the *PARASOL* polarization data from 1 August 2007, the MODIS C5M

model (smooth particles) for $D_{\text{eff}} = 60 \mu\text{m}$ provided a poor fit to the observations, while the model at $D_{\text{eff}} = 60 \mu\text{m}$ based on the GHM assuming severely roughened ice particles most improved the comparison with measurements. To determine whether the ice cloud optical models based on the GHM provide a match to observations over a range of D_{eff} that might be encountered in ice cloud retrievals, simulations were performed for optically thick ice clouds ($\tau = 5$) at $D_{\text{eff}} = 30, 50, 70,$ and $90 \mu\text{m}$, all with severely roughened particles. Figure 5 shows the results for all four cases. Although there is a slight variation with D_{eff} , the simulated polarized reflectances compare favorably to the *PARASOL* measurements.

The question we now address is whether an individual habit can be used instead of a habit mixture. Figure 6 shows the simulated polarized reflectance, again assuming $D_{\text{eff}} = 60 \mu\text{m}$ and $\tau = 5$ for each of the nine habits shown in Fig. 1. Interestingly, the hollow particles tend to most closely match with the observations, and the hollow bullet rosettes in particular do well. Plates have simulated polarized reflectances that are too large at small scattering angles from 60° to 120° , while solid columns and droxtals have polarized reflectance values that are too small over roughly the same range. Even

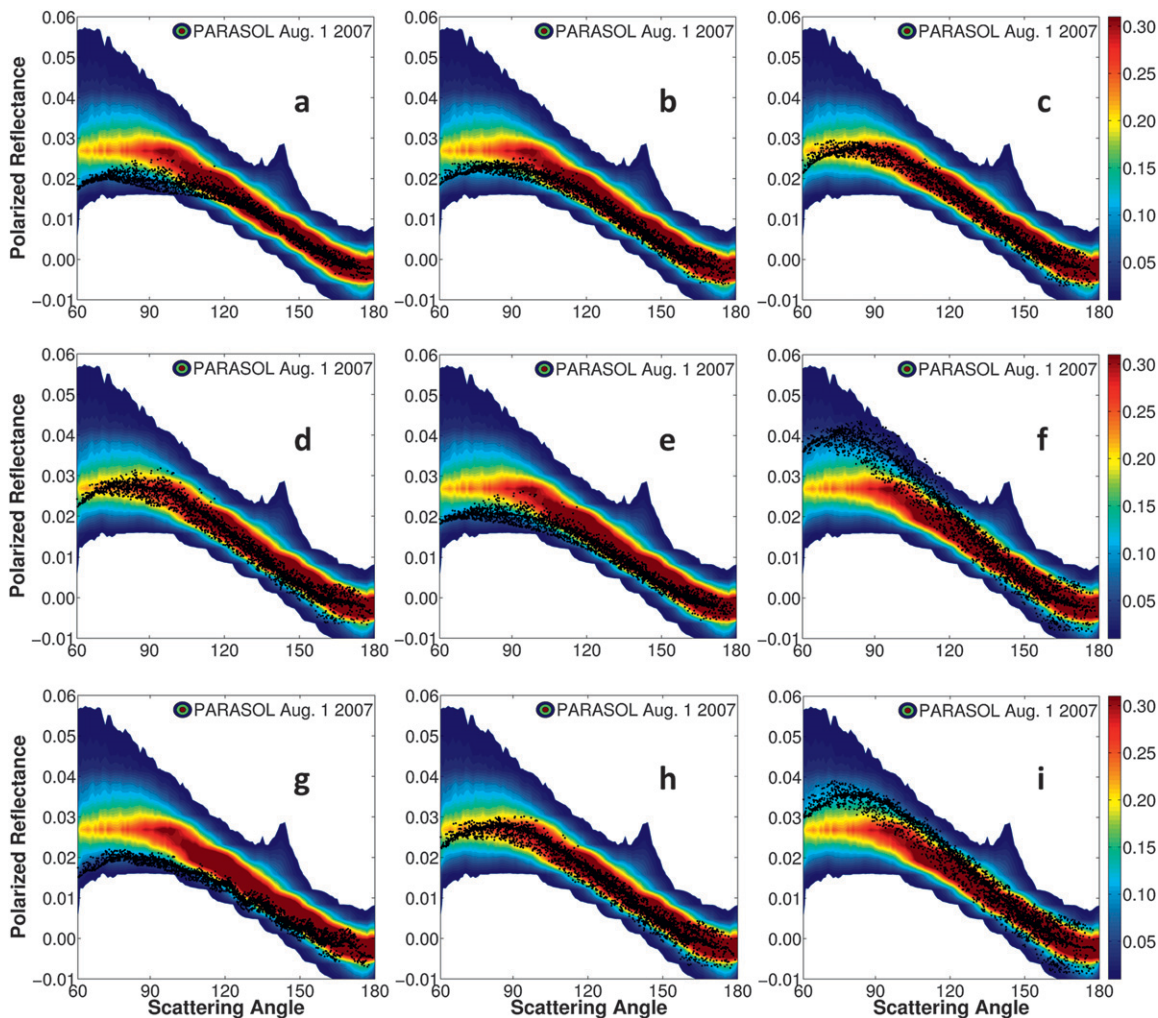


FIG. 6. Simulated polarized reflectance calculated using nine different single ice habits, all at an effective diameter of $60 \mu\text{m}$: (a) droxtal, (b) solid 3D bullet rosette, (c) hollow 3D bullet rosette, (d) hollow column, (e) solid column, (f) plate, (g) compact aggregate of columns, (h) small spatial aggregate of plates, and (i) large spatial aggregate of plates. An optically thick ($\tau = 5$) ice cloud is used in the simulation and the ice particles are severely rough. Color contours show the density of the *PARASOL* polarized reflectance data from 1 Aug 2007, and black dots are simulations.

though some single habits can provide a good fit to the observed *PARASOL* measurements when severe surface roughness is assumed, it is advantageous to use a habit mix to conserve ice mass, as was shown in Baum et al. (2005a) and Baran et al. (2009, 2011). The GHM model was shown in Baum et al. (2011) to compare well with the microphysical properties provided by in situ data, specifically with regard to ice water content (IWC) and median mass diameter.

The results of the SAD analysis for the general habit mix as well as several single habits are shown in Fig. 7 for $D_{\text{eff}} = 60 \mu\text{m}$. The desired result for a given model is that it should minimize the normalized relative spherical albedo differences. Additionally, the residual quantities should not have any strong angular dependence. When

a least squares linear fit is performed through the residual, the correlation coefficient should be high and the slope should be as small as possible, indicating no angular dependence. The top three panels in Fig. 7 illustrate the impact of surface roughening with the GHM models, indicating that it does reduce angular biases in cloud optical thickness retrievals. This is consistent with previous studies that showed that angular biases were reduced by randomizing the ice crystals in some fashion (Baran et al. 2001; Baran and C.-Labonnote 2006, 2007). The bottom three panels in Fig. 7 in combination with the top right for the severely roughened particle model illustrate the impact of particle habit distributions. It can clearly be seen that details of the habit distribution are somehow of second order when surface roughening is

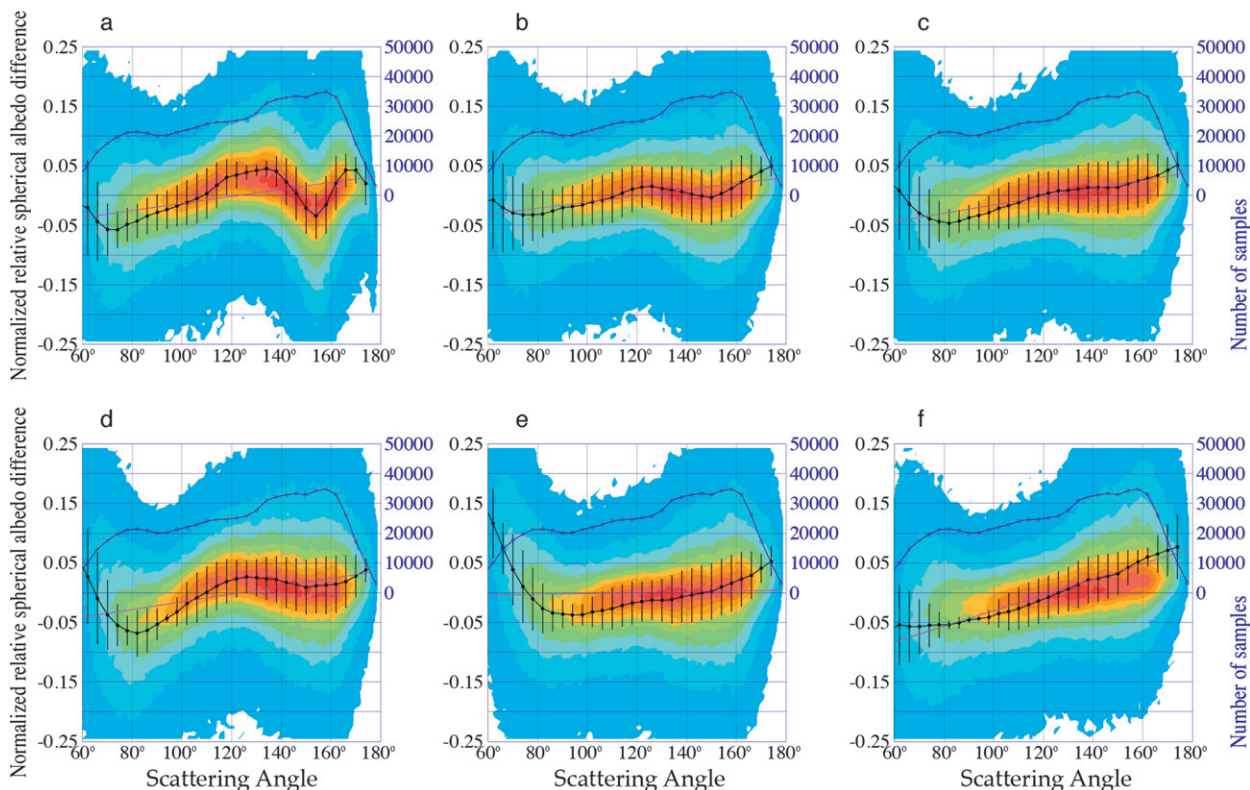


FIG. 7. Results of the relative SAD analysis for the GHM and selected single habits: (a) GHM smooth; (b) GHM moderately rough; (c) GHM severely rough; (d) solid column, severely rough; (e) solid 3D bullet rosette, severely rough; and (f) hollow 3D bullet rosette, severely rough. Color contours show the density of the observations normalized to the maximum value, and blue dots are the number of samples at that scattering angle (scale on the right). One day of global observations from 1 Aug 2007 is used.

introduced but some strong differences remain visible, especially at side scattering angles below 90° .

The top panel in Fig. 8 shows the RMS of relative spherical albedo differences over the full range of effective diameters for the models under consideration. All the models evaluated tend to provide comparable relative SAD RMSs over the two different days of data tested, with the results for 1 August 2007 shown here. The GHM tends to be slightly better at larger effective diameters in terms of RMS. The hollow bullet rosette and solid column (both severely roughened) have an almost-constant SAD RMS regardless of the effective diameter, and provide the smallest RMS for $D_{\text{eff}} \leq 30 \mu\text{m}$.

The middle and bottom panels in Fig. 8 show the slope of the linear regression performed through the SAD residual, as well as the linear correlation coefficient. The various models present significantly different patterns of behavior in terms of the slope as a function of effective diameter. The solid column (severely rough) has the least variation while the slope from the GHM actually changes sign when going from small to large D_{eff} . The linear correlation coefficients indicate, however, that the solid column still exhibits a significant

angular variability that is not present in the *PARASOL* observations. Similarly, the solid bullet rosette (severely roughened) has small slope values but the corresponding linear correlation coefficients are low, indicating that angular biases created by the model assumption are highly variable (i.e., not linearly correlated with the scattering angle).

4. Summary

This study investigates the fit of simulated polarized reflectance at $0.865 \mu\text{m}$ to *PARASOL* multiangle polarized reflectance observations using different ice habit mixtures and values of ice particle surface roughness. A spherical albedo difference test is used to determine the angular consistency of the ice models. The MODIS collection-5 ice habit mixture, a new general habit mixture, and individual habits are used to simulate polarized reflectances. The surface roughness can be smooth, moderately rough, or severely rough.

The MODIS C5M models result in a poor fit of the simulated polarized reflectances to the observed polarized reflectances, and add to the evidence that the

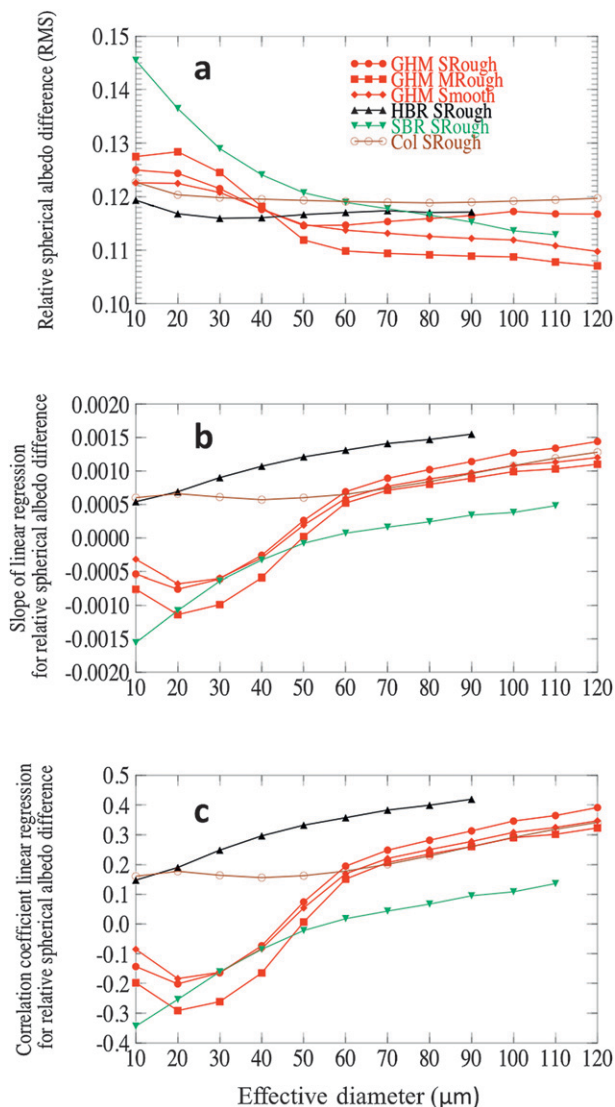


FIG. 8. (a) RMSs of relative SAD for the various models, (b) the slope of the linear regression for the relative spherical albedo differences, and (c) the correlation coefficients of the linear regression for the relative spherical albedo differences. One day of global observations from 1 Aug 2007 is used.

assumption of smooth particles may be inadequate for the global retrieval of ice properties. With the GHM, which uses three additional habits and has the habit fractions changing linearly with particle size, the assumption of smooth-faceted ice crystals also provides a poor comparison with *PARASOL*. As the roughening increases, however, the comparison of simulated to measured polarized reflectances improves across a range of effective diameters and scattering angles.

With bulk scattering models based on the GHM and severely roughened particles, the simulated to measured polarized reflectances remain comparable for a range of

effective diameter values from 30 to 90 μm. This range of D_{eff} values is encompassed from current MODIS retrievals (although these are based on smooth particles).

There are individual ice habits that can match the observed *PARASOL* polarized reflectance data, including hollow columns and hollow bullet rosettes. However, an ensemble mix of ice habits better matches the IWC and median mass diameter in situ data (Baum et al. 2005a; Baran et al. 2009, 2011). As cloud retrieval teams decide what bulk scattering models to adopt in future operational and research efforts, these results will hopefully provide useful guidance.

From the SAD analysis, it is difficult to decide which model is the best in all respects. It is clear that surface roughness does improve significantly the different metrics used to quantify the adequacy of a model in terms of minimizing systematic angular biases occurring when deriving cloud optical thickness. It should be noted that moderate roughening tends to provide smaller values of slope (i.e., less angular dependency) than severe roughening. Moderate roughening also gives slightly better relative SAD RMS values but at the same time does not yield as high a linear correlation as does severe roughening. It seems that the GHM has some advantages since it compares well with the SAD but includes some variations over a range of effective diameters. Hollow bullet rosettes and solid bullet rosettes tend to provide slightly worse results but are more homogeneous over the range of effective diameters.

With regard to the varying results over the effective diameter, it must be noted that a single unique model (habit + size) has been used to process the measured *PARASOL* data each time. No attempt has been made to select the best effective size for a given habit distribution, and in fact it would not be very surprising that the best microphysical model could indeed depend strongly on particle size.

Previous work by Knap et al. (2005) found that the imperfect hexagonal monocrystal and inhomogeneous hexagonal monocrystal models simulated adequately the polarized reflectance observed globally on 10 November 1996. The advantage of the GHM model considered in the current study is that it compares well to IWC and median mass diameter inferred from in situ microphysical data (Baum et al. 2011), and it also adequately simulates the global polarized reflectance observed on 1 August 2007.

From all the habit-based models considered in this study, the one that provides the best match to the polarized reflectance observations and gives reasonable results in the SAD analysis is the general habit mixture with severe particle roughening. It is suggested that this model would potentially be an adequate choice for

future global ice cloud retrievals using MODIS, and a significant improvement over the C5M models adopted for collection-5 operational processing.

Acknowledgments. We thank the ICARE Data and Services Center for providing access to the data used in this study and for tools used in the data processing. This study was supported by NASA Grants NNX10AL55G and NNX11AK37G. Bryan Baum and Ping Yang also acknowledge the support of NASA Grant NN11AF40G.

REFERENCES

- Baran, A. J., 2009: A review of the light scattering properties of cirrus. *J. Quant. Spectrosc. Radiat. Transfer*, **110**, 1239–1260.
- , and L. C.-Labonnote, 2006: On the reflection and polarization properties of ice cloud. *J. Quant. Spectrosc. Radiat. Transfer*, **100**, 41–54.
- , and —, 2007: A self-consistent scattering model for cirrus. I: The solar region. *Quart. J. Roy. Meteor. Soc.*, **133**, 1899–1912.
- , P. N. Francis, L. C.-Labonnote, and M. Doutriaux-Boucher, 2001: A scattering phase function for ice cloud: Tests of applicability using aircraft and satellite multi-angle multi-wavelength radiance measurements of cirrus. *Quart. J. Roy. Meteor. Soc.*, **127**, 2395–2416.
- , P. J. Connolly, and C. Lee, 2009: Testing an ensemble model of cirrus ice crystals using midlatitude in situ estimates of ice water content, volume extinction coefficient and the total solar optical depth. *J. Quant. Spectrosc. Radiat. Transfer*, **110**, 1579–1598.
- , —, A. J. Heymsfield, and A. Bansemmer, 2011: Using in situ estimates of ice water content, volume extinction coefficient, and the total solar optical depth obtained during the tropical ACTIVE campaign to test an ensemble model of cirrus ice crystals. *Quart. J. Roy. Meteor. Soc.*, **137**, 199–218.
- Baum, B. A., A. J. Heymsfield, P. Yang, and S. T. Bedka, 2005a: Bulk scattering properties for the remote sensing of ice clouds. Part I: Microphysical data and models. *J. Appl. Meteor. Climatol.*, **44**, 1885–1895.
- , P. Yang, A. J. Heymsfield, S. E. Platnick, M. D. King, Y. X. Hu, and S. T. Bedka, 2005b: Bulk scattering properties for the remote sensing of ice clouds. Part II: Narrowband models. *J. Appl. Meteor. Climatol.*, **44**, 1896–1911.
- , —, Y. X. Hu, and Q. Feng, 2010: The impact of ice particle roughness on the scattering phase matrix. *J. Quant. Spectrosc. Radiat. Transfer*, **111**, 2534–2549.
- , —, A. J. Heymsfield, C. G. Schmitt, Y. Xie, A. Bansemmer, Y.-X. Hu, and Z. Zhang, 2011: Improvements in shortwave bulk scattering and absorption models for the remote sensing of ice clouds. *J. Appl. Meteor. Climatol.*, **50**, 1037–1056.
- Buriez, J. C., and Coauthors, 1997: Cloud detection and derivation of cloud properties from POLDER. *Int. J. Remote Sens.*, **18**, 2785–2813.
- Chepfer, H., G. Brogniez, and Y. Fouquart, 1998: Cirrus clouds' microphysical properties deduced from POLDER observations. *J. Quant. Spectrosc. Radiat. Transfer*, **60**, 375–390.
- C.-Labonnote, L., G. Brogniez, J. C. Buriez, and M. Doutriaux-Boucher, 2001: Polarized light scattering by inhomogeneous hexagonal monocrystals: Validation with ADEOS-POLDER measurements. *J. Geophys. Res.*, **106**, 12 139–12 153.
- de Haan, J. F., P. B. Bosma, and J. W. Hovenier, 1987: The adding method for multiple scattering calculations of polarized light. *Astron. Astrophys.*, **183**, 371–391.
- Deschamps, P., F. M. Breon, M. Leroy, A. Podaire, A. Bricaud, J. C. Buriez, and G. Seze, 1994: The POLDER mission: Instrument characteristics and scientific objectives. *IEEE Trans. Geosci. Remote Sens.*, **32**, 598–615.
- Doutriaux-Boucher, M., J.-C. Buriez, G. Brogniez, L. C.-Labonnote, and A. J. Baran, 2000: Sensitivity of retrieved POLDER directional cloud optical thickness to various ice particle models. *Geophys. Res. Lett.*, **27**, 109–112.
- Fougnie, B., G. Bracco, B. Lafrance, C. Ruffel, O. Hagolle, and C. Tinel, 2007: PARASOL in-flight calibration and performance. *Appl. Opt.*, **46**, 5435–5451.
- Hu, Y. X., B. Wielicki, B. Lin, G. Gibson, S. C. Tsay, K. Stamnes, and T. Wong, 2000: δ -fit: A fast and accurate treatment of particle scattering phase functions with weighted singular-value decomposition least-squares fitting. *J. Quant. Spectrosc. Radiat. Transfer*, **65**, 681–690.
- Joseph, J. H., W. J. Wiscombe, and J. A. Weinman, 1976: Delta-Eddington approximation for radiative flux-transfer. *J. Atmos. Sci.*, **33**, 2452–2459.
- Knap, W. H., L. C.-Labonnote, G. Brogniez, and P. Stamnes, 2005: Modeling total and polarized reflectances of ice clouds: Evaluation by means of POLDER and ATSR-2 measurements. *Appl. Opt.*, **44**, 4060–4073.
- Liou, K. N., 1986: Influence of cirrus clouds on weather and climate processes: A global perspective. *Mon. Wea. Rev.*, **114**, 1167–1198.
- Nazaryan, H., M. P. McCormick, and W. P. Menzel, 2008: Global characterization of cirrus clouds using CALIPSO data. *J. Geophys. Res.*, **113**, D16211, doi:10.1029/2007JD009481.
- Tomasi, C., V. Vitale, B. Petkov, A. Lupi, and A. Cacciari, 2005: Improved algorithm for calculations of Rayleigh-scattering optical depth in standard atmospheres. *Appl. Opt.*, **44**, 3320–3341.
- Yang, P., and K. N. Liou, 1998: Single-scattering properties of complex ice crystals in terrestrial atmosphere. *Contrib. Atmos. Phys.*, **71**, 223–248.
- , L. Bi, B. A. Baum, K. N. Liou, G. W. Kattawar, M. Mishchenko, and B. Cole, 2013: Spectrally consistent scattering, absorption, and polarization properties of atmospheric ice crystals at wavelengths from 0.2 to 100 μm . *J. Atmos. Sci.*, **70**, 330–347.